Neoclassical impurity flux in presence of turbulent generated poloidal asymmetries and pressure anisotropy

Peter Donnel, Xavier Garbet, Yanick Sarazin, Virginie Grandgirard, Nicolas Bouzat, Elisabetta Caschera, Guilhem Dif-Pradalier, Philippe Ghendrih, Camille Gillot, Guillaume Latu, et al.

Neoclassical impurity flux in presence of poloidal asymmetries

P. Donnel[1], X. Garbet[1], Y. Sarazin[1], V. Grandgirard[1], N. Bouzat[2], E.Caschera[1], G. Dif-Pradalier[1], P. Ghendrih[1], C. Gillot[3], G. Latu[1], C. Passeron[1]

August 8, 2018

Abstract

Poloidal asymmetries of impurities are commonly observed experimentally. Density asymmetry is already known to impact significantly neoclassical prediction of impurity flux. In this article, the effect of impurity pressure asymmetry and anisotropy on the neoclassical flux of impurity is derived analytically. This prediction is compared with results coming from a simulation performed with the gyrokinetic code GYSELA, featuring both turbulent and neoclassical transports. A fair agreement is found between the analytical prediction and the result of the simulation. On the special case which is considered, the effect of impurity pressure asymmetry and anisotropy are shown to play a predominant role on the neoclassical impurity transport.

1 Introduction

Impurity transport is an issue of utmost importance for fusion. One reason is the choice of tungsten for ITER divertor. Indeed high-Z materials are only partially ionized in the plasma core, so that they can lead to prohibitive radiative losses even at low concentrations, and impact dramatically plasma performance and stability. On-axis accumulation of tungsten has been widely observed in tokamaks [1, 2]. While the very core impurity peaking is generally attributed to neoclassical effects, turbulent transport could well dominate in the gradient region at ITER relevant collisionality. The transport of helium ashes and medium-Z impurities also results from both neoclassical and turbulent transport. Up to recently, first principles simulations of corresponding fluxes were performed with different dedicated codes, implicitly assuming that both transport channels are separable and therefore additive. One of the key questions is whether this assumption is valid.

Preliminary simulations obtained with the gyrokinetic code GYSELA [3] have shown evidence of a neoclassical-turbulence synergy for impurity transport [4]. However no clear theoretical explanation was given, although poloidal asymmetries were pointed out as critical players. New simulations have been done using a new and more accurate collision operator [5] and improved boundary conditions [6]. The new collision operator allows in particular the isotropisation of the pressure thanks to the inclusion of derivatives with respect to the adiabatic invariant μ. This version of GYSELA has been successfully benchmarked against neoclassical theory. In particular, analytical predictions of the pinch velocity and screening factor are recovered.

The new simulations confirm the neoclassical-turbulence synergy and allow identification of a mechanism that underlie this synergy. The new simulations have indeed shown strong poloidal asymmetries attributed to the presence of turbulence. Poloidal asymmetries of the impurity density is known to impact significantly the neoclassical flux of impurity [7, 8, 9]. In this article we generalize this approach by including the effect of poloidal asymmetries of pressure and anisotropies in the neoclassical prediction of impurity flux. This new prediction is then convincingly compared to results

coming from the GYSELA code. It is stressed that pressure asymmetries can lead to a significant modification of the neoclassical flux of impurities.

2 Impurity flux in presence of poloidal asymmetries

2.1 Structure of the impurity flow

In this section, a stationary ($\frac{\partial}{\partial t} = 0$) and an axisymmetric ($\frac{\partial}{\partial \varphi} = 0$) system is considered. We neglect the effect of the turbulence generated Reynolds stress. Poloidal asymmetries of the main ion are neglected whereas those of the impurity are kept. The physical origin of these poloidal asymmetries is not discussed in this section, so that they are assumed to be given inputs in the model. The magnetic field considered is of the form

$$\mathbf{B} = I(\psi)\nabla\varphi + \nabla\varphi \times \nabla\psi$$

and the system of coordinates is (ψ, θ, φ). The following results do not depend on the choice of poloidal angle θ. The momentum equation for impurities reads

$$N_Z Ze\left(\mathbf{E} + \mathbf{V}_Z \times \mathbf{B}\right) - \nabla \cdot \mathbf{\Pi}_Z + \mathbf{R}_{Zi} = 0 \tag{1}$$

where the pressure tensor $\mathbf{\Pi}_Z$ reads

$$\mathbf{\Pi}_Z = P_{\perp Z}\mathbf{I} + \Pi_{\parallel Z}\mathbf{bb}$$

and $\Pi_{\parallel Z} = P_{\parallel Z} - P_{\perp Z} + N_Z m_z V_{\parallel Z}^2$. It then readily appears that

$$\nabla \cdot \mathbf{\Pi}_Z = \nabla P_{\perp Z} + \Pi_{\parallel Z}\boldsymbol{\kappa} + \left[(\mathbf{B}\cdot\nabla)\left(\frac{\Pi_{\parallel Z}}{B}\right)\right]\mathbf{b}$$

Where $\boldsymbol{\kappa} = -\mathbf{b} \times (\nabla \times \mathbf{b})$ is the field curvature. Taking $\frac{\mathbf{B}}{Ze}\times(1)$ and noting that $\mathbf{B} \times \mathbf{R}_{Zi} = 0$, the flux reads

$$\mathbf{\Gamma}_Z = \Gamma_{\parallel Z}\mathbf{b} + N_Z\frac{\mathbf{B}}{B^2} \times \nabla\phi + \frac{\mathbf{B}}{ZeB^2} \times \nabla \cdot \mathbf{\Pi}_Z \tag{2}$$

Noting that $\nabla\phi = \frac{\partial\phi}{\partial\psi}\nabla\psi + \frac{\partial\phi}{\partial\theta}\nabla\theta$ and $\nabla P_{\perp Z} = \frac{\partial P_{\perp Z}}{\partial\psi}\nabla\psi + \frac{\partial P_{\perp Z}}{\partial\theta}\nabla\theta$, and using the identity

$$\frac{\mathbf{B}}{B^2} \times \nabla\psi = I\frac{\mathbf{B}}{B^2} - R^2\nabla\varphi$$

one gets

$$\mathbf{\Gamma}_Z = K_Z\mathbf{B} - N_Z\Omega_Z R^2\nabla\varphi + \frac{\Pi_{\parallel Z}}{ZeB}\left(\mathbf{b}\times\boldsymbol{\kappa}\right) + \left(N_Z\frac{\partial\phi}{\partial\theta} + \frac{1}{Ze}\frac{\partial P_{\perp Z}}{\partial\theta}\right)\frac{\mathbf{B}}{B^2} \times \nabla\theta$$

All quantities depend on (ψ, θ). The following definitions have been introduced $\Omega_Z = \frac{\partial\phi}{\partial\psi} + \frac{1}{N_Z Ze}\frac{\partial P_{\perp Z}}{\partial\psi}$

$$K_Z = \frac{\Gamma_{\parallel Z}}{B} + \frac{I}{B^2}N_Z\Omega_Z$$

$$V_{\parallel Z} = \frac{K_Z B}{N_Z} - \frac{I}{B}\Omega_Z$$

2.2 Determination of K_Z

$K_Z(\psi,\theta)$ is constrained by the equation $\nabla\cdot\mathbf{\Gamma}_Z=0$, which reads

$$(\mathbf{B}\cdot\nabla)\,K_Z+\nabla\cdot\tilde{\mathbf{\Gamma}}_Z=0 \tag{3}$$

where

$$\tilde{\mathbf{\Gamma}}_Z=\frac{\Pi_{\parallel Z}}{ZeB}\left(\mathbf{b}\times\boldsymbol{\kappa}\right)+\left(N_Z\frac{\partial\phi}{\partial\theta}+\frac{1}{Ze}\frac{\partial P_{\perp Z}}{\partial\theta}\right)\frac{\mathbf{B}}{B^2}\times\nabla\theta$$

We recall here the expression of the divergence of a vector $\boldsymbol{V}$ that does not depend on φ

$$\frac{\nabla\cdot\boldsymbol{V}}{\mathbf{B}\cdot\nabla\theta}=\frac{\partial}{\partial\psi}\left(\frac{\boldsymbol{V}\cdot\nabla\psi}{\mathbf{B}\cdot\nabla\theta}\right)+\frac{\partial}{\partial\theta}\left(\frac{\boldsymbol{V}\cdot\nabla\theta}{\mathbf{B}\cdot\nabla\theta}\right)$$

Using the following relations

$$(\mathbf{b}\times\boldsymbol{\kappa})\cdot\nabla\psi=I\mathbf{B}\cdot\nabla\theta\frac{\partial}{\partial\theta}\left(\frac{1}{B}\right)$$

$$(\mathbf{b}\times\boldsymbol{\kappa})\cdot\nabla\theta=-I\mathbf{B}\cdot\nabla\theta\frac{\partial}{\partial\psi}\left(\frac{1}{B}\right)$$

$$(\mathbf{B}\times\nabla\theta)\cdot\nabla\psi=-I\mathbf{B}\cdot\nabla\theta$$

one then obtains

$$\begin{aligned}\frac{\nabla\cdot\tilde{\mathbf{\Gamma}}_Z}{\mathbf{B}\cdot\nabla\theta}=&\frac{\partial}{\partial\theta}\left[\frac{1}{B}\frac{\partial}{\partial\psi}\left(\frac{I\Pi_{\parallel Z}}{ZeB}\right)\right]\\&-\frac{I}{ZeB^2}\frac{\partial}{\partial\psi}\left[N_ZZe\frac{\partial\phi}{\partial\theta}+\frac{\partial P_{\perp Z}}{\partial\theta}+B\frac{\partial}{\partial\theta}\left(\frac{\Pi_{\parallel Z}}{B}\right)\right]\end{aligned} \tag{4}$$

One can note that in the absence of poloidal asymmetries, $\nabla\cdot\tilde{\mathbf{\Gamma}}_Z=0$, therefore K_Z depends on ψ only. Now let us note that the parallel projection of the momentum Eq.(1) implies that

$$\mathbf{B}\cdot\nabla\theta\left[N_ZZe\frac{\partial\phi}{\partial\theta}+\frac{\partial P_{\perp Z}}{\partial\theta}+B\frac{\partial}{\partial\theta}\left(\frac{\Pi_{\parallel Z}}{B}\right)\right]=BR_{\parallel Zi} \tag{5}$$

where we have used the fact that $\mathbf{b}\cdot\boldsymbol{\kappa}=0$. If the friction force is subdominant locally, then Eq.(5) implies that the second term of Eq.(4) is vanishing. Therefore equation (3) becomes

$$\frac{\partial}{\partial\theta}\left[K_Z+\frac{1}{B}\frac{\partial}{\partial\psi}\left(\frac{I\Pi_{\parallel Z}}{ZeB}\right)\right]=0 \tag{6}$$

It is quite remarkable that no solubility problem arises when the friction force is neglected. The function K_Z then reads $K_Z=K_{Z0}(\psi)+K_{Z1}(\psi,\theta)$, where

$$K_{Z0}=\langle K_Z\rangle$$

$$K_{Z1}=-\frac{1}{B}\frac{\partial}{\partial\psi}\left(\frac{I\Pi_{\parallel Z}}{ZeB}\right)+\left\langle\frac{1}{B}\frac{\partial}{\partial\psi}\left(\frac{I\Pi_{\parallel Z}}{ZeB}\right)\right\rangle \tag{7}$$

Here, the bracket denotes the flux surface average :

$$\langle f\rangle=\frac{\oint\frac{d\theta d\varphi}{\mathbf{B}\cdot\nabla\theta}f}{\oint\frac{d\theta d\varphi}{\mathbf{B}\cdot\nabla\theta}}$$

2.3 Neoclassical flux

If the main ion is in the banana regime and the impurity in the Pfirsch-Schlütter regime, it can be shown that the friction force reads [10]

$$R_{\|Zi} = m_z \nu_{Zi} \left\{ -N_Z \frac{T_i}{eB} \frac{I}{L_\psi} + B \left(N_Z u - K_Z \right) \right\} \tag{8}$$

where $\frac{1}{L_\psi} = \frac{1}{L_{\psi,i}} + \frac{1}{L_{\psi,z}}$ with $\frac{1}{L_{\psi,i}} = \frac{\partial P_i}{P_i \partial \psi} - \frac{3}{2} \frac{\partial T_i}{T_i \partial \psi}$ and $\frac{1}{L_{\psi,z}} = -\frac{1}{T_i Z N_z} \frac{\partial P_{\perp Z}}{\partial \psi}$. $L_{\psi,i}$ is a flux function whereas $L_{\psi,z}$ is a function of ψ and θ. u is a flux function that can be approximated in the limits of large aspect ratio $\epsilon \ll 1$ and trace impurity $\frac{n_z Z^2}{n_i} \ll 1$ by $u \simeq -0.33 \frac{f_c I}{e \langle B^2 \rangle} \frac{\partial T_i}{\partial \psi}$ [10]. Note that ν_{Zi} is also flux function. Using Eq.(5), while keeping the friction force leads to the solubility constraint

$$\left\langle \frac{B R_{\|Zi}}{N_Z} \right\rangle = \left\langle \frac{\mathbf{B} \cdot \nabla \theta}{N_Z} \left[\frac{\partial P_{\perp Z}}{\partial \theta} + B \frac{\partial}{\partial \theta} \left(\frac{\Pi_{\|Z}}{B} \right) \right] \right\rangle \tag{9}$$

Combining Eq.(7), Eq.(8) and Eq.(9), one finds

$$\begin{aligned} K_{Z0} = & -\frac{T_i I}{e} \langle \frac{1}{L_\psi} \rangle \left\langle \frac{B^2}{N_Z} \right\rangle^{-1} + u \left\langle B^2 \right\rangle \left\langle \frac{B^2}{N_Z} \right\rangle^{-1} \\ & + \left\langle \frac{B}{N_Z} \frac{\partial}{\partial \psi} \left(\frac{I \Pi_{\|Z}}{ZeB} \right) \right\rangle \left\langle \frac{B^2}{N_Z} \right\rangle^{-1} - \left\langle \frac{1}{B} \frac{\partial}{\partial \psi} \left(\frac{I \Pi_{\|Z}}{ZeB} \right) \right\rangle \\ & - \frac{1}{m_z \nu_{Zi}} \left\langle \frac{\mathbf{B} \cdot \nabla \theta}{N_Z} \left[\frac{\partial P_{\perp Z}}{\partial \theta} + B \frac{\partial}{\partial \theta} \left(\frac{\Pi_{\|Z}}{B} \right) \right] \right\rangle \left\langle \frac{B^2}{N_Z} \right\rangle^{-1} \end{aligned} \tag{10}$$

These expression of K_{Z0} can then be plugged into the friction force to calculate the impurity radial flux $\langle \mathbf{\Gamma}_Z \cdot \nabla \psi \rangle = -\frac{I}{Ze} \left\langle \frac{R_{\|Zi}}{B} \right\rangle$, i.e.

$$\begin{aligned} \langle \mathbf{\Gamma}_Z \cdot \nabla \psi \rangle = & -\frac{I}{Ze} m_z \nu_{Zi} \left\{ -\frac{T_i}{e} \frac{I}{L_{\psi,i}} \left(\left\langle \frac{N_Z}{B^2} \right\rangle - \frac{1}{\left\langle \frac{B^2}{N_Z} \right\rangle} \right) - \frac{T_i I}{e} \left(\left\langle \frac{N_z}{B^2 L_{\psi,z}} \right\rangle - \left\langle \frac{1}{L_{\psi,z}} \right\rangle \frac{1}{\left\langle \frac{B^2}{N_z} \right\rangle} \right) \right. \\ & \left. + u \left(\langle N_Z \rangle - \frac{\langle B^2 \rangle}{\left\langle \frac{B^2}{N_Z} \right\rangle} \right) + \left\langle \frac{1}{B} \frac{\partial}{\partial \psi} \left(\frac{I \Pi_{\|Z}}{ZeB} \right) \right\rangle - \frac{\left\langle \frac{B}{N_Z} \frac{\partial}{\partial \psi} \left(\frac{I \Pi_{\|Z}}{ZeB} \right) \right\rangle}{\left\langle \frac{B^2}{N_Z} \right\rangle} \right\} \\ & - \frac{I}{Ze} \frac{1}{\left\langle \frac{B^2}{N_Z} \right\rangle} \left\langle \frac{\mathbf{B} \cdot \nabla \theta}{N_Z} \left[\frac{\partial P_{\perp Z}}{\partial \theta} + B \frac{\partial}{\partial \theta} \left(\frac{\Pi_{\|Z}}{B} \right) \right] \right\rangle \end{aligned} \tag{11}$$

The first and third terms of the r.h.s are identical to Eq.(10) of [7] for which only poloidal density asymmetries are considered. The second term corresponds to a simple diffusion which is often neglected but can become important when impurity peaking is strong. The fourth and fifth terms are entirely controlled by K_{Z1}, and represent a modification of the friction force due to the impurity pressure anisotropy and finite parallel Mach number of the impurity. Finally the last term can be seen as a modification of the banana-plateau flux. Note that it is independent of the interspecies collisionality and will therefore dominate for low collisionality regimes.

3 Comparison with results from gyrokinetic simulations

The goal of this section is to assess the relative importance of the various contributions in the neoclassical prediction derived in the previous section (11) using the results of a simulation performed with the code GYSELA. In this simulation, poloidal asymmetries are self-generated by turbulence. This simulation considers deuterium as the main species and tungsten with a fixed charge state

$Z = 40$ as a trace impurity $\left(\alpha = \frac{N_z Z^2}{N_i} \sim 10^{-3}\right)$. An adiabatic response is taken for electrons. The size of the machine simulated is fixed by the dimensionless parameter $\rho_{\star,i} = \frac{\rho_i}{a} = \frac{1}{190}$ where ρ_i is the Larmor radius of a thermal ion at mid-radius. GYSELA uses a simplified geometry with circular magnetic surfaces characterized by the inverse aspect ratio $\frac{R_0}{a} = 4.4$ and the safety factor profile $q(r) = 1.5 + 1.3\exp\left(2.5\log\left(\frac{r}{a}\right)\right)$. The collisionality of the main ion species at mid-radius is $\nu_i^\star = 0.1$, which is therefore in the banana regime. The impurity collisionality at mid-radius is $\nu_z^\star \simeq \sqrt{\frac{2m_i}{m_z}} Z^2 \nu_i^\star \simeq 24$. The impurity is in the Pfirsch-Schlütter regime. The two ion species start with identical density and temperature profiles $\frac{d\ln n_s(r)}{dr} = -2.2\cosh^{-2}\left(\frac{\rho-0.5}{0.04}\right)$ and $\frac{d\ln T_s(r)}{dr} = -6\cosh^{-2}\left(\frac{\rho-0.5}{0.04}\right)$. To approach steady state, an isotropic source of energy is added [3]. Its amplitude depends only on the radius. Finally, the outer boundary condition is ensured via a penalization technique [6].

The phase-space grid is well resolved $\left(N_r, N_\theta, N_\varphi, N_{v_\parallel}, N_\mu\right) = (512, 1024, 32, 127, 64)$ and the time step $\Delta t\omega_{ci} = 16$ chosen to resolve accurately both the turbulent and collisional time scales. Because of this high resolution and the presence of two species, the numerical cost of this simulation is very large. In order to reduce this cost, the following strategy has been used : in a first stage, the code is run without impurity until quasi steady state. The impurity is added in a second stage. Despite this strategy, the convergence of the simulation toward a quasi steady state in the presence of impurity still requires several millions of CPU hours. For this reason, the quasi steady state is not reached in the simulation which is presented. Non stationarity is therefore important, in particular for the parallel force balance (5). As the model derived in the previous section is valid only for steady-state, a perfect match between the neoclassical flux given by the code and the theoretical prediction is not expected. Nevertheless, it is shown that the model (11) gives the good order of magnitude for the impurity flux coming from GYSELA.

In the considered GYSELA simulation, the poloidal asymmetries are self-generated by turbulence. The poloidal asymmetry of the tungsten density Fig.1 is of the order of 20% and can be expressed simply in the form $N_z = \langle N_z\rangle(\psi)\left[1 + \delta(\psi)\cos\theta + \Delta(\psi)\sin\theta\right]$. The knowledge of $\delta(\psi)$ and $\Delta(\psi)$ then allows one to compute the impact of density asymmetries on the first and third terms of (11), which correspond to terms already present in the literature [7]. Indeed, one can show that these terms take the following simple expressions:

$$\left\langle \frac{N_Z}{B^2} \right\rangle - \frac{1}{\left\langle \frac{B^2}{N_Z} \right\rangle} = \frac{\langle N_z\rangle(\psi)}{\langle B^2\rangle}\left[2\epsilon(\epsilon+\delta) + \frac{\delta^2+\Delta^2}{2}\right] \tag{12}$$

$$\langle N_Z\rangle - \frac{\langle B^2\rangle}{\left\langle \frac{B^2}{N_Z} \right\rangle} = \langle N_Z\rangle\left[\epsilon\delta + \frac{\delta^2+\Delta^2}{2}\right] \tag{13}$$

Here, poloidal asymmetry contributions come from the δ and Δ terms only. Fig.2 shows the radial shape of (12) and (13) for the GYSELA simulation. It readily appears that both expressions remain close to their value at $\delta = \Delta = 0$, i.e. in the absence of any poloidal asymmetry. More precisely, the impact of the tungsten density poloidal asymmetries on these expressions is moderate in the deep core and weak in the outer part of the simulation.

Conversely, Fig.4 shows that the poloidal asymmetry of both impurity pressure and pressure anisotropy provide a significant contribution to the impurity flux, especially in the inner part of the simulation. This results comes from the spatially strongly localized nature of $P_{\perp Z}$ and $\Pi_{\parallel Z}$, as evident from Fig.3. Due to this local character, the terms proportional to the spatial derivatives of these two quantities are important in Eq.(11).

The final test consists in comparing the neoclassical flux coming from GYSELA defined as $\langle \mathbf{\Gamma}_Z \cdot \nabla\psi\rangle = -\frac{I}{Ze}\left\langle \frac{R_{\parallel Zi}}{B} \right\rangle$, with the neoclassical prediction Eq.(11). This comparison is depicted on Fig.5. The right order of magnitude is recovered, although there is some mismatch around $\rho = 0.2$.

Figure 1: Left: poloidal asymmetry of the impurity density. Right: reconstruction of the poloidal asymmetry with $\delta(\psi)$ and $\Delta(\psi)$

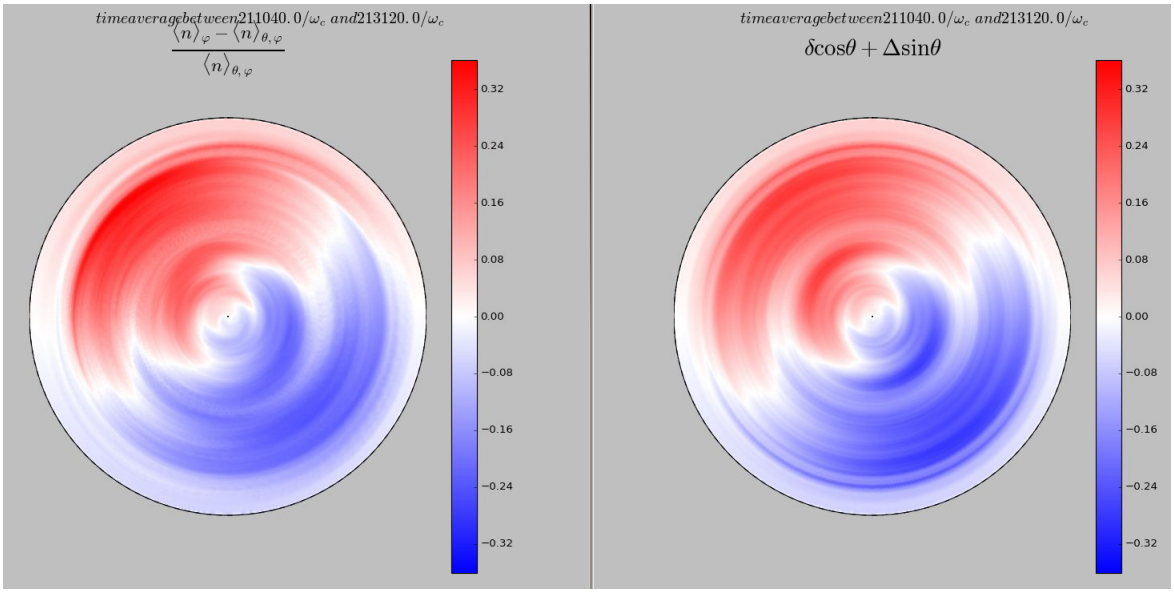

Figure 2: Radial shape of Eq.(12) in red and Eq.(13) in green. The blue curve represents the radial shape of Eq.(12) in the absence of poloidal asymmetry of the impurity density, i.e. for $\delta = \Delta = 0$.

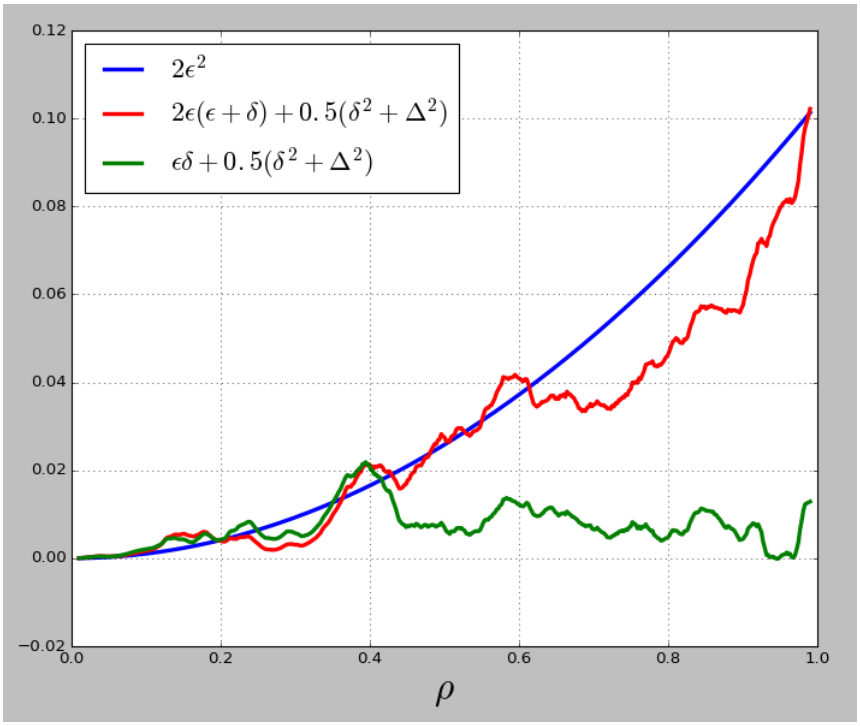

Figure 3: Top: anisotropy of the impurity pressure. Bottom left: Energy in the parallel direction. Bottom right: CGL tensor divided by the magnetic field.

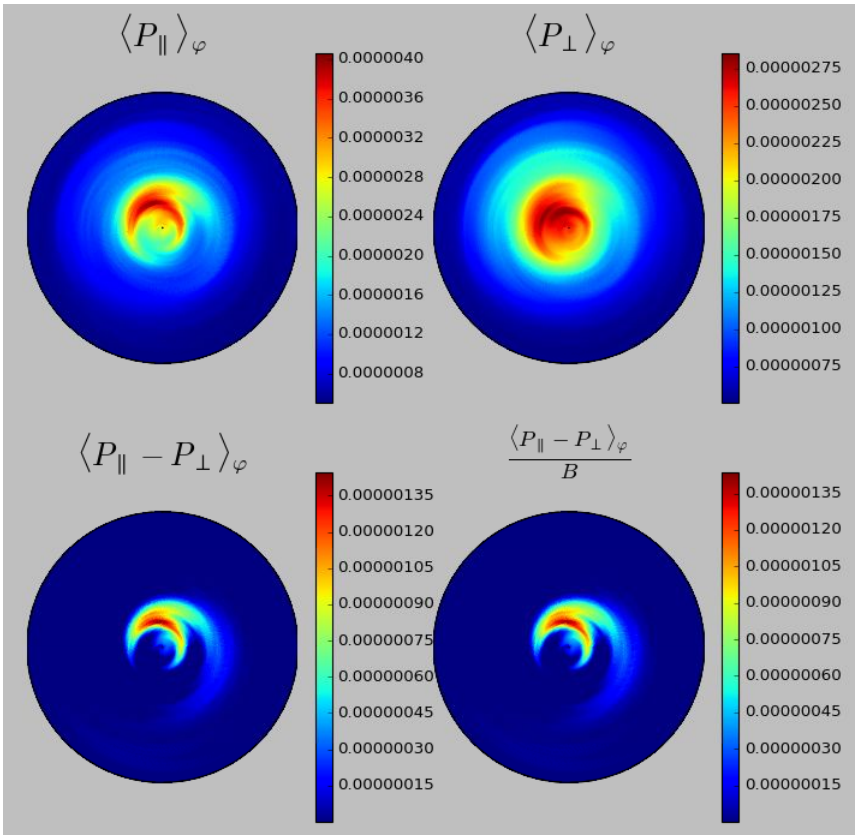

Importantly, the agreement is lost if the poloidal asymmetries of the pressure are not taken into account. The mismatch could come from different limitations of the model developed in the part II.

For instance, the non stationarity and the turbulent Reynolds stress contributions have been completely neglected. To assess the level of non stationarity, it is enlightening to look at the toroidal momentum conservation equation for species s

$$\partial_t L_{\varphi,s} = Ze\left(\Gamma_s^\Psi - \Gamma_{E,s}^\Psi\right) - \partial_\psi \Pi_{\varphi,s}^\Psi + \left\langle \frac{I}{B} R_{\parallel,s} \right\rangle_\Psi$$

with

$$\begin{aligned}
L_{\varphi,s} &= \left\langle m_s \int d^3\boldsymbol{v} u_\varphi F_s \right\rangle \\
\Pi_{\varphi,s}^\Psi &= m_s \left\langle \int d^3\boldsymbol{v} u_\varphi F_s \left(\boldsymbol{v}_{E\times B} + \boldsymbol{v}_{D,s}\right)\cdot\nabla\Psi \right\rangle \\
\Gamma_{E,s}^\Psi &= \left\langle \int d^3\boldsymbol{v} F_s \partial_\varphi \bar{\phi} \right\rangle \\
\Gamma_s^\Psi &= \langle \boldsymbol{\Gamma}_{\perp,s}\cdot\nabla\Psi \rangle_\Psi
\end{aligned}$$

Where $u_\varphi = \frac{I}{B} v_\parallel$ and $\bar{\phi}$ is the gyro-averaged electric potential. $R_{\parallel,s}$ is the total collisional drag force on the s species $R_{\parallel,s} = \sum_{s'} R_{\parallel,ss'}$. This conservation for the GYSELA simulation is plotted on Fig.6. First notice that toroidal momentum conservation (black line) is not perfect. However, the imbalance remains small compared to any of the other contributions. This means that firm conclusions can be safely drawn. Secondly, the non stationarity (red curve) appears to be important. This is the sign that the quasi stationarity state is not reached. The non stationarity is mostly compensated by the impurity flux and the turbulence-driven Reynolds stress (blue curve). The collisional friction (green curve) is sub-dominant almost everywhere.

Figure 4: Components of the neoclassical flux. Red and blue curves: effect of ion gradients. Cyan curve: effect of the impurity gradients. These three quantities are sensitive to the density asymmetry. Green and black curves: terms due to pressure asymmetry and anisotropy.

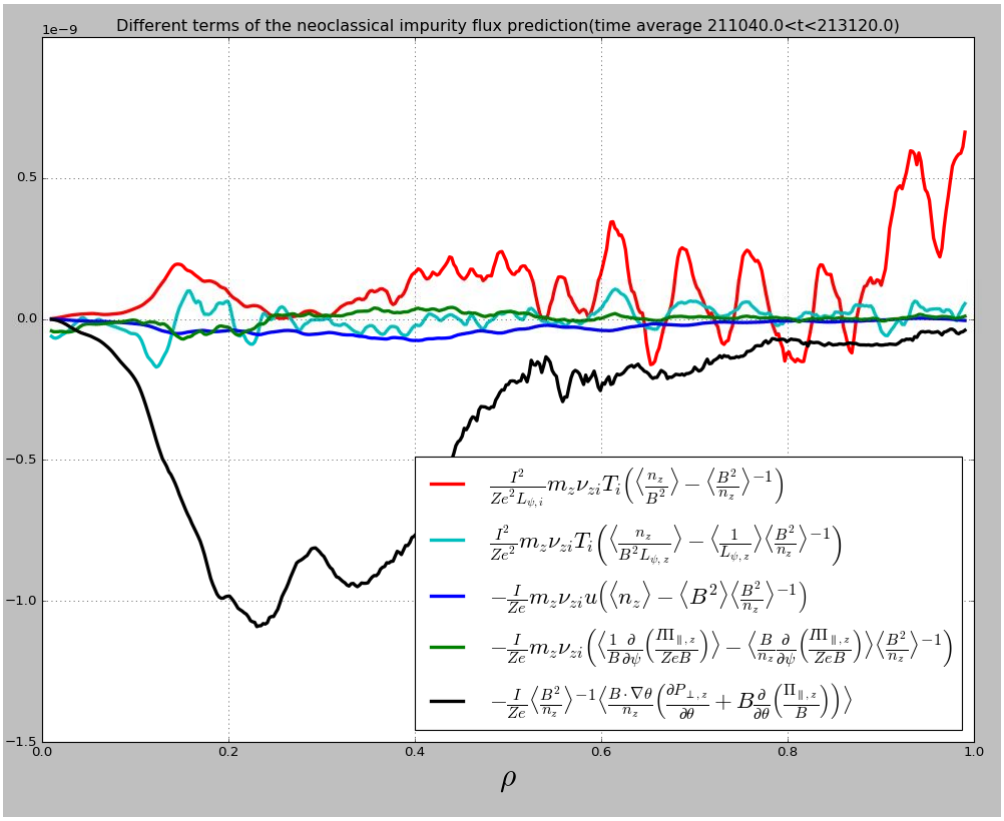

Figure 5: Comparison of the theoretical prediction of the neoclassical radial impurity flux (red) with the GYSELA flux (blue).

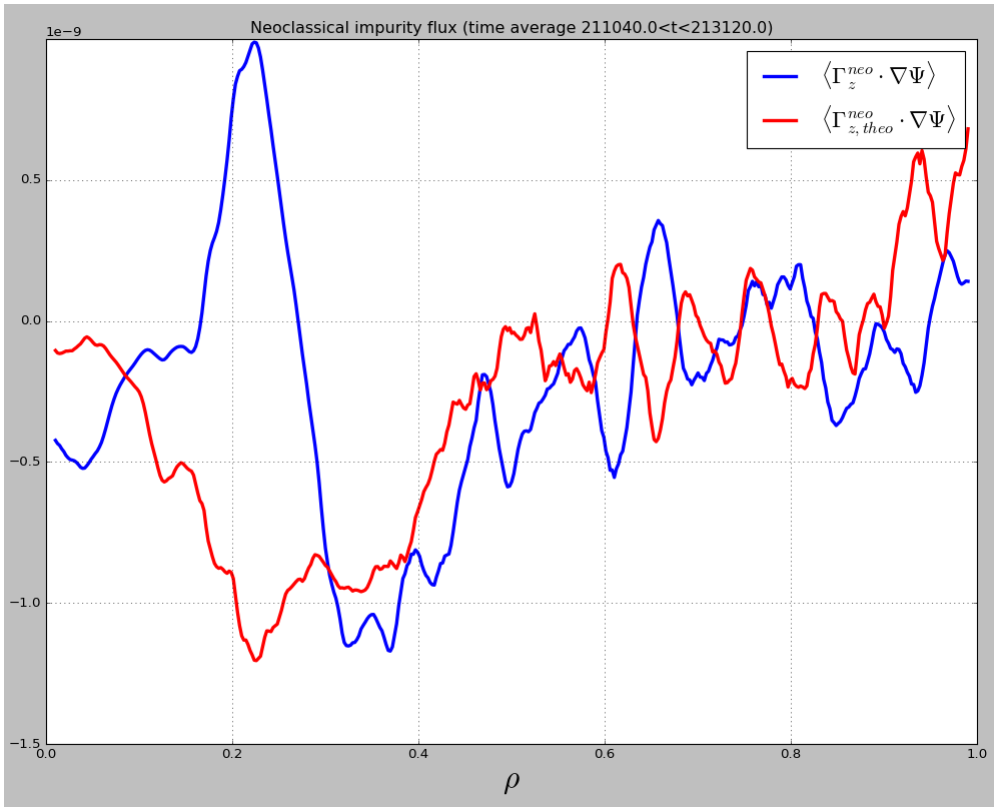

Figure 6: Toroidal momentum conservation. The non stationarity (red) is mostly compensated by the flux of particle (blue). The collisional exchange of momentum (green) is sub-dominant almost everywhere. Total conservation of toroidal momentum (dotted black) is reached within a few percents.

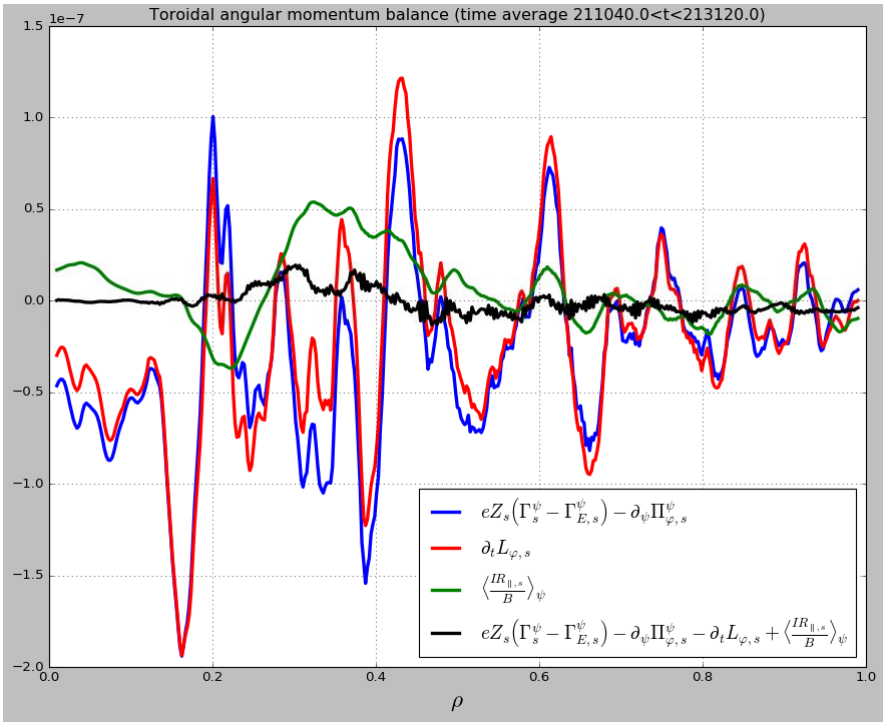

Another limitation of the model concerns the main ion. It is indeed implicitly assumed in the part II that the main ion species can be modeled by an isotropic Maxwellian distribution. Due to turbulence and the low collisionality of the main ion species, this assumption could easily break down. An illustration of this deviation from the Maxwellian for the main ion is given by the pressure anisotropy of the main ion represented on the Fig.7. Eventhough the ion anisotropy is not poloidally localized, it is of the same order of magnitude as the one of the impurity. The effect of the departure from the Maxellian could be even stronger on the parallel ion flux as it depends from higher order moments of the distribution function. The inclusion of such kinetic modification of the neoclassical flux of impurity is out of the scope of the present article but could reveal necessary for a better understanding of the synergy between turbulent and neoclassical mechanisms in the impurity transport framework.

4 Conclusion

The impact of both poloidal asymmetry and anisotropy of impurity pressure on the neoclassical impurity flux have been derived analytically. These corrections can reveal important when considering realistic cases, where pressure poloidal asymmetry and anisotropy can be generated by turbulence and/or sources. In particular, accounting for these corrections to the standard neoclassical prediction could reveal critical in the perspective of impurity control by external heating systems. On the theoretical point of view, this work provides a clear mechanism for synergy between neoclassical and turbulent processes in the context of impurity transport. Importantly, these predictions are found in fair agreement with a dedicated and highly resolved GYSELA simulation – featuring both turbulent and neoclassical transports, where the correction terms appear to have a major contribution.

Figure 7: Flux surface average of the pressure anisotropy of the ion (blue) and the impurity (red)

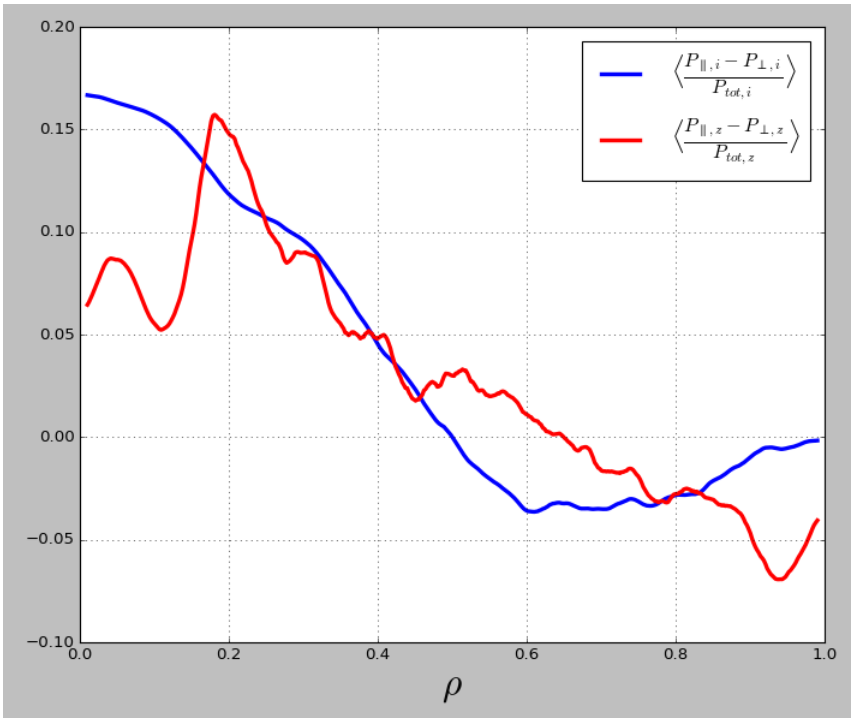

Acknowledgments

This work was granted access to the national HPC resources of OCCIGEN/CINES and European machine dedicated to fusion Marconi/CINECA. This work has been carried out within the framework of the EUROfusion Consortium and has received funding from the Euratom research and training program 2014-2018 under grant agreement No 633053 for the project WP17-ENR-CEA-02. This work was also supported by the Energy oriented Center of Excellence (EoCoE), grant agreement number 676629, funded within the Horizon2020 framework of the European Union. The views and opinions expressed herein do not necessarily reflect those of the European Commission.

References

[1] E. Joffrin, M. Baruzzo, M. Beurskens, C. Bourdelle, S. Brezinsek, J. Bucalossi, P. Buratti, G. Calabro, C.D. Challis, M. Clever, J. Coenen, E. Delabie, R. Dux, P. Lomas, E. de la Luna, P. de Vries, J. Flanagan, L. Frassinetti, D. Frigione, C. Giroud, M. Groth, N. Hawkes, J. Hobirk, M. Lehnen, G. Maddison, J. Mailloux, C.F. Maggi, G. Matthews, M. Mayoral, A. Meigs, R. Neu, I. Nunes, T. Puetterich, F. Rimini, M. Sertoli, B. Sieglin, A.C.C. Sips, G. van Rooij, I. Voitsekhovitch, and JET-EFDA Contributors. First scenario development with the jet new iter-like wall. *Nuclear Fusion*, 54(1):013011, 2014.

[2] T Pütterich, R Dux, R Neu, M Bernert, M N A Beurskens, V Bobkov, S Brezinsek, C Challis, J W Coenen, I Coffey, A Czarnecka, C Giroud, P Jacquet, E Joffrin, A Kallenbach, M Lehnen, E Lerche, E de la Luna, S Marsen, G Matthews, M-L Mayoral, R M McDermott, A Meigs, J Mlynar, M Sertoli, G van Rooij, the ASDEX Upgrade Team, and JET EFDA Contributors. Observations on the w-transport in the core plasma of jet and asdex upgrade. *Plasma Physics and Controlled Fusion*, 55(12):124036, 2013.

[3] V. Grandgirard, J. Abiteboul, J. Bigot, T. Cartier-Michaud, N. Crouseilles, G. Dif-Pradalier, Ch. Ehrlacher, D. Estève, X. Garbet, Ph. Ghendrih, G. Latu, M. Mehrenberger, C. Norscini, Ch. Passeron, F. Rozar, Y. Sarazin, E. Sonnendrucker, A. Strugarek, and D. Zarzoso. A 5d gy-

rokinetic full-f global semi-lagrangian code for flux-driven ion turbulence simulations. *Computer Physics Communications*, 207:35 – 68, 2016.

[4] D. Estève, Y. Sarazin, X. Garbet, V. Grandgirard, S. Breton, P. Donnel, Y. Asahi, C. Bourdelle, G. Dif-Pradalier, C. Ehrlacher, C. Emeriau, P. Ghendrih, C. Gillot, G. Latu, and C. Passeron. Self-consistent gyrokinetic modeling of neoclassical and turbulent impurity transport. *Nuclear Fusion*, 2017.

[5] P. Donnel, X. Garbet, Y. Sarazin, V. Grandgirard, Y. Asahi, N. Bouzat, E. Caschera, G. Dif-Pradalier, C. Ehrlacher, P. Ghendrih, C. Gillot, G. Latu, and C. Passeron. A multi-species collisional operator for full-f global gyrokinetics codes : Numerical aspects and verification with the gysela code. *Submitted to Computer Physics Communications*, 2018.

[6] G. Dif-Pradalier, G. Hornung, X. Garbet, Ph. Ghendrih, V. Grandgirard, G. Latu, and Y. Sarazin. The exb staircase of magnetised plasmas. *Nuclear Fusion*, 57(6):066026, 2017.

[7] C Angioni and P Helander. Neoclassical transport of heavy impurities with poloidally asymmetric density distribution in tokamaks. *Plasma Physics and Controlled Fusion*, 56(12):124001, 2014.

[8] F J Casson, C Angioni, E A Belli, R Bilato, P Mantica, T Odstrcil, T Pütterich, M Valisa, L Garzotti, C Giroud, J Hobirk, C F Maggi, J Mlynar, and M L Reinke. Theoretical description of heavy impurity transport and its application to the modelling of tungsten in jet and asdex upgrade. *Plasma Physics and Controlled Fusion*, 57(1):014031, 2015.

[9] M Romanelli and M Ottaviani. Effects of density asymmetries on heavy impurity transport in a rotating tokamak plasma. *Plasma Physics and Controlled Fusion*, 40(10):1767, 1998.

[10] T Fülöp and P Helander. Nonlinear neoclassical transport in a rotating impure plasma with large gradients. 6:3066–3075, 08 1999.